Microfluidic schemes using electrical and capillary forces

2008 J. Phys.: Conf. Ser. 142 012054

(http://iopscience.iop.org/1742-6596/142/1/012054)

Journal of Physics: Conference Series **142** (2008) 012054 doi:10.1088/1742-6596/142/1/012054

Microfluidic schemes using electrical and capillary forces

TB Jones

Department of Electrical and Computer Engineering, University of Rochester, Rochester, NY (USA)

email: jones@ece.rochester.edu

Abstract. The laboratory-on-a-chip (LOC) and indeed virtually all the technology of microTAS (micro-total-analysis systems) rely upon some microfluidic subsystem to control, transport, and manipulate small liquid masses. The most promising of these subsystems use electrical forces, which have the advantages of voltage-based control and dominance over gravity and capillarity in the 10 to 10^3 micron diameter range. Gravity is usually ignorable on this scale, but the interactions of electrical and capillary forces are more complex. In particular, microstructures can be designed to exploit this interplay for the cases of electrowetting on dielectric-coated electrodes (EWOD) and liquid dielectrophoresis (DEP). The complementary nature of the two effects explains the operation of droplet-based microfluidic systems in general, and the so-called DEP droplet dispenser in particular.

1. Introduction

Electrostatic forces depend strongly on the size scale at which one intends to exploit them. In particular, most microelectromechanical systems (MEMS) are capacitive transducers where controllable electrical forces readily dominate over other forces. The same is true for micro-total-analysis systems (microTAS), such as the laboratory-on-a-chip (LOC) and other related schemes, where electrical forces are used to manipulate liquids. The dominance of electrostatics in MEMS and microTAS in the 10 to 10^3 micron range, and its contrasting ineffectiveness above a few millimeters, exemplifies what Feynman characterized as *lack of symmetry* of the physical laws as dimensions are changed [1]. Scaling an electrostatic system downward drastically alters the relative magnitudes of forces, leading to distinctive dynamics not observed in larger systems. Good examples of such unfamiliar behavior are found in microfluidic devices, where electrical forces and capillarity are the two main influences on the hydrostatics and hydrodynamics. This paper considers the sometimes competitive, but more often complementary natures of electrostatic and capillary/wetting forces on the microscale. While the scaling issue is central to this subject, the specific focus here is certain hydrostatic and hydrodynamic phenomena driven by electrowetting and/or liquid dielectrophoresis (DEP) and/or surface tension forces. More general treatments of the scaling issue may be found elsewhere [2,3,4].

2. Electromechanical microfluidic mechanisms

The mechanisms of electric-field mediated microfluidics can be divided loosely into two categories: electrohydrodynamic (EHD) and electromechanical. EHD mechanisms, including electro-osmotic pumping and electroconvection, involve bulk interactions between unbalanced electric charge and

electric fields. In contrast, electromechanical mechanisms, the focus of this paper, involve forces on conductors or dielectric bodies.

2.1. Electrowetting on dielectric-coated electrodes

Discovered over a century ago, electrowetting has recently gained prominence as a practical, microfluidic mechanism. Its most common realization, electrowetting-on-dielectric or EWOD, uses segmented, individually addressable, optically transparent electrodes coated thinly with a dielectric, typically 1 to 10 μm thick. EWOD has two observable manifestations: a contact angle effect, exploited in liquid lenses, and a translational force effect, useful in the laboratory-on-a-chip and other μTAS schemes [5].

1.1.1. The contact angle effect A sessile droplet of moderately conductive liquid on a dielectric-coated electrode forms a variable capacitor. Upon application of voltage, the droplet spreads and increases the capacitance. Refer to fig. 1. The Coulombic force acting on induced charges at the liquid/air interface near the contact line causes this spreading. If $\theta_E(V = 0) = \theta_o$, the Lippmann equation predicts the contact angle [6].

$$\cos[\theta_E(V)] - \cos\theta_o = \varepsilon_d \varepsilon_o V^2 / 2\gamma d \qquad (1)$$

where d and ε_d are the thickness and dielectric constant of the insulating layer, respectively, γ = liquid/air surface tension, and $\varepsilon_o = 8.854 \cdot 10^{-12}$ F/m is the free space permittivity.

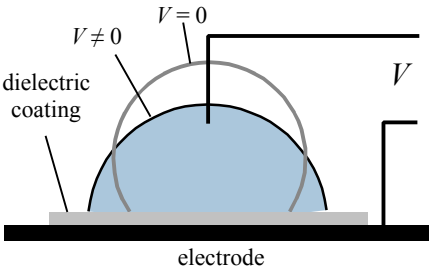

Fig. 1. The EWOD effect displayed by a sessile droplet on a dielectric-coated electrode. At low Bond number, the droplet maintains the profile of a spherical segment.

The dimensionless Bond number, $Bo = (\rho g D^2 / 4\gamma)^{0.5}$, where ρ = liquid density, $g = 9.81$ m/s^2, and D = droplet diameter, compares gravity to surface tension. If $Bo \ll 1$, the sessile droplet profile is well-approximated as a spherical segment, in which case, the voltage-dependent contact angle, $\theta_E(V)$, serves as a single description of the droplet profile. Thus, when $Bo \ll 1$ aqueous droplets of diameter $D \leq$ ~500 μm (~0.1 μliter) will always take a spherical profile. Another dimensionless modulus, $Ew = \varepsilon_d \varepsilon_o V^2 / 2\gamma d$, provides a measure of the electrically-induced spreading effect. Setting $Ew = 0.1$ yields an estimate for the voltage required to achieve an observable reduction of the contact angle. For a water droplet (γ = 0.072 N/m, $\rho = 10^3$ kg/m^3) on a coating of dielectric thickness $d/\varepsilon_d \sim 1$ μm, the calculated voltage is $V \approx 40$ Volts.

1.1.2. *Contact angle saturation* The practical application of Eq. (1) is limited in practice because contact angle saturation clamps the electrowetting effect well before the implicit $\theta_E = 0°$ limit is reached. Saturation severely restricts the application of electrowetting; apparent contact angles below ~60° are seldom achieved [7]. The phenomenon is not very well-understood, though there exist some plausible mechanisms: (i) charge injection into the dielectric from the liquid; (ii) EHD-driven droplet spraying from the contact line; and (iii) corona discharge. One should note that none of these mechanisms inherently exclude the others. We can investigate the threshold conditions corresponding to (i) charge injection and (ii) air corona by calculating appropriate field strength values by solving Eq. (1) for the electric field in the dielectric layer.

$$E_{layer} = V/d = \left(2\gamma(\cos\theta_E - \cos\theta_o)/\varepsilon_d \varepsilon_o d\right)^{0.5} \qquad (2)$$

Using $\varepsilon_d = 2.5$, $d = 2.5$ μm, γ = 0.072 N/m, $(\theta_E)_{max} = 60°$, and $\theta_o = 90°$ in Eq. (2) gives $E_{layer} = 3.6 \cdot 10^7$ V/m, corresponding to applied voltage $V = 90$ V. Comparing this result to typical breakdown limits tests the likelihood of charge injection. For the spin-on or dip-coated polymers typically used as coatings in EWOD structures (such as SU-8™ and Teflon-AF™) the breakdown field is $(E_{layer})_{max} \approx 2 \cdot 10^7$ V/m. Because the calculated value for E_{layer} exceeds this threshold, one would expect that charge injection intervenes before the contact angle gets down to 60°. The other electrical mechanism

possible linked to saturation is corona, the onset of which is ordinarily assessed by comparing an estimate of the local electric field in air to the well-known air breakdown limit: $E_{\text{breakdown}} = 3\bullet10^6$ V/m. The field in the air, around the edges of the rivulet is difficult to estimate, but a rough value can be obtained using $E_{\text{air}} \approx \varepsilon_{\text{d}} E_{\text{layer}}$. Then, with the previously stipulated parameters, we have $E_{\text{air}} \approx 9\bullet10^7$ V/m, strongly suggesting that corona occurs at a voltage far lower than the threshold for charge injection. This outcome may seem compelling, yet it is important to bear in mind that, because the dielectric strength of spin-coated layers is notoriously difficult to characterize and because of uncertainty in estimating the value of E_{layer} reliably, a definitive conclusion about the relative importance of charge injection and corona remains illusive, making identification of the mechanism responsible for contact angle saturation all the more difficult.

1.1.3. *The translational force effect* Some very promising electric-field-based microfluidic devices use dielectric-coated, individually addressable electrodes. It is the convention to group such schemes with the droplet-spreading phenomenon revealed in fig. 1. As a result, models for these devices often use the apparent contact angle defined in Eq. (1) to estimate the translational force responsible for the liquid motion. An alternative is to formulate the electrical force using the methods of classical electromechanics. In particular, the so-called force of electrical origin can be expressed in terms of capacitance $C(x)$ [8].

$$f_x^{\text{e}} = \tfrac{1}{2} V^2 \, dC/dx \tag{3}$$

where x is a mechanical degree of freedom that measures the position of the liquid mass, capacitance has the form $C(x) \approx \varepsilon_{\text{d}} \varepsilon_0 \, w x / d$, w = structure width, and other quantities are previously defined. The electromechanical interpretation possesses the clear advantage that it can be generalized to cover both EWOD and liquid DEP regimes in a single, frequency-dependent model. This is so because changes in the contact angle are not needed either to explain or to estimate the electrical force responsible for center-of-mass motions important to microfluidics. In fact, liquid DEP lacks any natural interpretation based on changes in the contact angle for the simple reason that the contact does not change significantly. One may conclude that the center-of-mass forces observed in EWOD microfluidics are not in fact causatively coupled to contact angle reduction.

1.2. Liquid dielectrophoresis

In the absence of free charge or electrostriction, the ponderomotive force per unit volume on a liquid is $\overline{F}^{\text{e}} = \tfrac{1}{2} E^2 \nabla \varepsilon$. A dielectric liquid mass responds to this force, first by collecting in regions where the imposed field magnitude $|E_{\text{o}}|$ is maximized and then by configuring itself with its free surfaces primarily tangential to $\overline{E}_{\text{o}}$.

1.2.1. *The Pellat experiment* The Pellat experiment depicted in fig. 2a exemplifies the important principles of liquid DEP [9]. The liquid rises against gravity between vertical, parallel electrodes in response to the DEP and capillarity forces, which are here additive.

$$h = (\varepsilon - \varepsilon_0) E_{\text{o}}^2 / 2\rho g + 2\gamma \cos\theta_{\text{o}} / \rho g s \tag{4}$$

$E_{\text{o}} = V/s$ is the essentially uniform electric field and the contact angle θ_{o} is the same quantity defined by Eq. (1). Eq. (4) suggests a new dimensionless modulus, $Be \equiv (\varepsilon - \varepsilon_0) s E_{\text{o}}^2 / 4\gamma \cos\theta_{\text{o}}$, comparing DEP to capillarity. Choosing $E_{\text{o}} = 10^6$ V/m as a safe upper limit for the electric field to avoid air breakdown, plus $\theta_{\text{o}} = 80°$, $s = 500$ μm, and values typical for insulating, organic liquids ($\varepsilon = 3$, $\gamma = 0.015$ N/m), we get $Be \approx 0.85$, indicating that capillarity

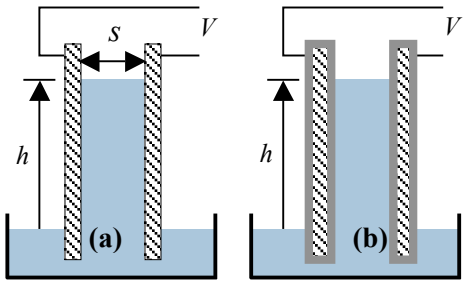

Fig. 2. Pellat apparatus with parallel, vertical electrodes separated by spacing s and dipped into liquid. (a) For insulating, dielectric liquids, bare electrodes are used. (b) For conductive liquids, Pellat apparatus is modified by uniformly coating electrodes with layer having dielectric constant ε_{d} and thickness $d << s$.

and DEP are roughly comparable. The nominal dielectric height-of-rise for this set of parameters is h ≈ 1 mm. If we instead assume the liquid is aqueous (ε = 80, γ = 0.072 N/m), then Be ≈ 7.1. Now, the DEP force can dominate over capillary. The height-of-rise increases to h ≈ 36 mm.

Modified Pellat experiment Coating the electrodes of the Pellat apparatus with a thin dielectric layer (d = thickness, ε_d = dielectric constant) facilitates study of the translational EWOD effect for aqueous liquids exploited in microTAS. See fig. 2b. Because the liquid is conductive, the entire voltage drop occurs across the dielectric coatings. The new expression for height-of-rise is [10]

$$h = \varepsilon_d \varepsilon_0 V^2 / 4\rho g s d + 2\gamma \cos\theta_0 / \rho g s \qquad (5)$$

The form of the electric Bond number must be changed to $Be' = \varepsilon_d \varepsilon_0 V^2 / 8\gamma \cos\theta_0 d$. Substituting the previously used parameter including the upper limit for the field strength in the layer, $V/d = 2 \cdot 10^7$ V/m, and θ_0 = 80° into Eq. (5), Be' ≈ 0.22, indicating that the capillary force predominates if the charge injection mechanism is limiting.

1.3. Relationship of EWOD and liquid DEP

The EWOD and liquid DEP microfluidics are intimately related through the frequency of the applied voltage that drives these mechanisms. A relatively simple lumped parameter model incorporating capacitances and resistances to represent the liquid and dielectric layers can be formulated to predict the frequency-dependent force [10]. Based on the RC circuit model, the critical frequency f^* that divides these limiting cases is

$$f^* = \sigma / [2\pi\varepsilon_0 (\varepsilon + \varepsilon_d s/2d)] \qquad (6)$$

where σ = liquid conductivity. At frequencies below f^*, conduction virtually shorts out the electric field within the liquid, so that the entire voltage drop occurs in the dielectric coatings; on the other hand, at frequencies above f^*, the electric field permeates the liquid as is typical in liquid DEP. Using s = 500 μm, d = 2.5 μm, and ε_d = 2.5, and further assuming the liquid to be an aqueous medium, ε = 80, σ = 10^{-3} S/m, Eq. (6) gives f^* ~ 31 kHz as the frequency dividing EWOD and DEP microfluidic actuation.

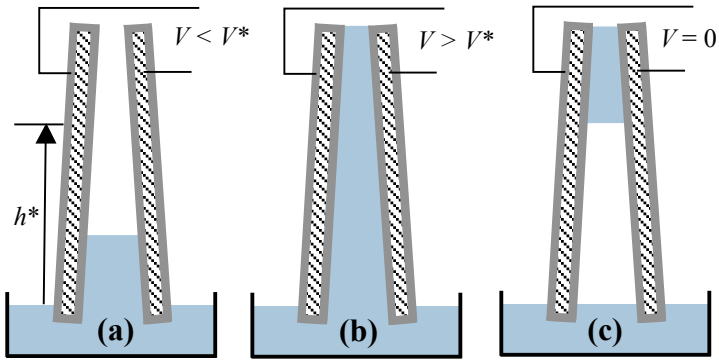

Fig. 3. Bifurcation phenomenon with spatially-varying electrode structure. (a) Rising voltage is below threshold of bifurcation, that is, $V < V^*$ and $h < h^*$. (b) Rising voltage is above threshold of bifurcation, $V > V^*$, and liquid has jumped discontinuously to the top from height h^*. (c) With decreasing voltage, the column first pinches in at height h^* and thus a portion of the liquid is trapped at the top. Surface tension can hold it indefinitely in this configuration with V = 0. This hysteretic behavior has interesting potential applications in precision microfluidic dispensing.

2. Interplay of electrical forces and capillarity

It is not difficult to design microfluidic structure where electrical forces dominate over capillarity but, because the voltage can be modulated, capillary forces can still be exploited effectively. The two examples described in the following sections illustrate such an interplay.

2.1. Electrohydrostatic bifurcation structures

Fig. 3 shows a bifurcation effect with spatially-varying electrodes that is observed when the ratio of the electrode spacing at the bottom and at the top is large enough. As voltage V is increased from zero, the liquid column rises monotonically until, at a predicable height $h = h^*$, corresponding to a voltage threshold V^*, the column jumps spontaneously to the top. When voltage is then reduced, the

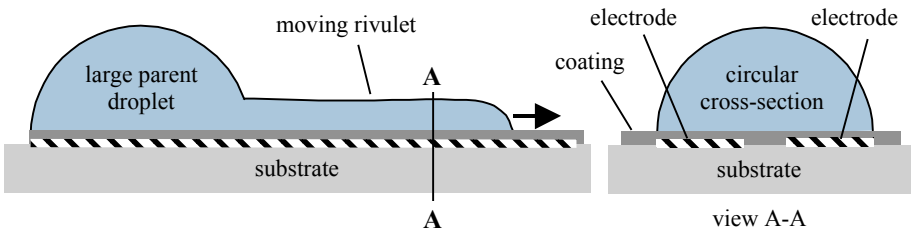

Fig. 4. Side and (enlarged) cross-sectional views of microfluidic DEP actuation and droplet dispenser uses parallel, coplanar strip electrodes patterned on an insulating substrate, then coated with dielectric and hydrophobic layers.

column first pinches off at h^* and the trapped liquid mass remains at the top, held in place by capillarity even when voltage is removed altogether. Surface tension also influences the pinch-off dynamics. This hysteretic behavior is frequency-dependent, manifesting low-frequency (EWOD) and high-frequency (liquid DEP) limits [11], in a fashion similar to the modified Pellat experiment shown in fig. 2b. A similar hydrostatic bifurcation phenomenon is predicted for conductive liquids rising between parallel electrodes if d, the thickness of the dielectric is tapered so as to vary gradually from thickest at the bottom to thinnest at the top.

2.2. Dispensing sessile droplets on a substrate

Fig. 4 shows side and cross-sectional views of a liquid DEP-actuated droplet dispenser. The parallel, coplanar electrodes, fabricated on an insulating substrate, are coated with thin dielectric/hydrophobic layers. Upon application of AC voltage, a liquid rivulet emerges from a droplet placed manually at one end of the structure and flows rapidly (at speeds up to ~50 cm/s) along the structure to the other end, where it stops and establishes electrohydrostatic equilibrium.

One may compare the DEP and capillary forces to find the condition where the electrical force should indeed suppress the capillary instability by taking the ratio of the normal Maxwell stress at the semi-circular liquid/air interface to the Laplace pressure, i.e., $(\varepsilon - 1)\varepsilon_0 V^2 / 2\pi^2 R\gamma$, where R = radius of the cross-section of the rivulet. For calculation purposes, we choose water for the liquid and let the cross-sectional width of the electrode structure dimension be $D = 2R = 100$ μm. As an electrical constraint, we assume the azimuthal electric field strength tangent to the free surface of the rivulet is limited by the breakdown strength of air, that is, $V/\pi R = 3 \bullet 10^6$ V/m. Then, the value of the above ratio is ~2.2, which means that the DEP force competes with or dominates capillarity.

As long as the electric field is present, the rivulet maintains a semicircular cross-section, but when the field is removed, the rivulet immediately deforms into a wavy filament and quickly (~10^{-2} s) pinches off into regularly spaced, sessile droplets along the structure [12]. This hydrostatic instability, depicted in fig. 5, is driven by surface tension, which takes over when the electrical DEP force is removed. Despite apparent differences between a free liquid jet and a sessile rivulet, the observed dominant wavelength λ very closely matches Rayleigh's model for the cylindrical jet, including his prediction of a most-unstable wavelength [13]. This result is also consistent with an analysis and supporting experiments using molten wax beads on a heated surface [14].

It is important to note that this critical wavelength determines both the spacing between the droplets and their ultimate volume.

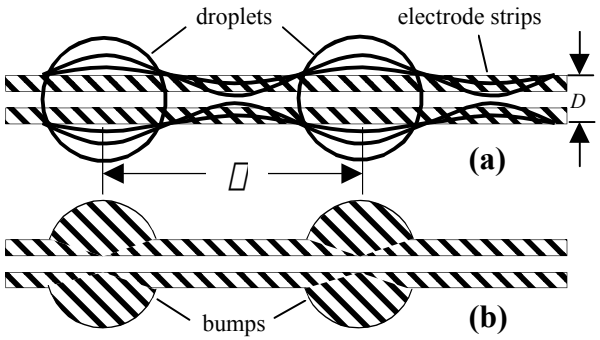

Fig. 5. Top view of basic liquid DEP actuator with coplanar strip electrodes on insulating substrate. (a) Evolution of capillary-driven instability leads to formation of sessile droplets, where λ is the fastest growing wavelength from Rayleigh's hydrodynamic theory. (b) Periodic bumps at spacing λ promote uniform, precise droplet formation.

3. Conclusion

Droplet-based microfluidic systems actuated by electrostatics have promising applications in the laboratory-on-a-chip. The principal mechanisms of interest are electrowetting on dielectric substrates

and liquid dielectrophoresis. These electromechanical mechanisms, offering continuous voltage-modulation as well as on/off control, dominate gravity and compete with capillarity on the microscale. The ordering of these forces, can be established by considering dimensionless moduli, among which are the Bond number, comparing gravity and capillarity, and others that measure the relative strength of electrical and capillary forces.

Depending on the specific microfluidic application, capillarity can be suppressed by electrical forces or exploited to manage liquid volumes from picoliters to microliters. One illustrative example of such a scheme is a liquid DEP droplet dispenser. This scheme uses the electrical force to distribute aqueous media in the form of long, static rivulets, and then, after removal of the voltage, exploits the familiar capillary-driven, hydrodynamic surface instability to break up the rivulet into droplets. In microsystems such as the laboratory-on-a-chip, these droplets might serve as aliquots of analyte for subsequent microbiological diagnostics or biochemical protocols. A similar interplay of capillarity and liquid DEP can be exploited to achieve rapid on/off flow control of dielectric liquids in coating and marking applications [15]. In these and other droplet-based microfluidic schemes, the control capability stems from the mismatch of the relatively stronger electromechanical and relatively weaker capillary effects.

Acknowledgment

R. Ahmed, C. Bailey, S. Bei, M. Gunji, and K-L. Wang obtained the videos and data upon which the paper has been based. The National Science Foundation (USA), NexPress Solutions, Inc., Center for Electronic Imaging Science and Laboratory for Laser Energetics (University of Rochester) supported this research. The author acknowledges gratefully a six-month fellowship from the Engineering and Physical Science Research Council (UK) at Southampton University during 2005.

References

[1] Feynman R 1965 *The Character of Physical Law* (Cambridge, MA (USA): MIT Press) p 95.
[2] Trimmer WSN 1989 *Sensors Actuators*, **19** 267.
[3] Jones TB 2003 Electrostatics on the Microscale *Electrostatics 2003*: Institute of Physics (UK), (Edinburgh, UK, April 2003).
[4] Jones TB 2003 *IEE Proc. Nanobiotechnology* **150** 39.
[5] Pollack MG, Fair RB, and Shenderov AD, 2000 *Appl. Phys. Lett.* **77** 1725; Lee J, Moon JH, Fowler J, Schoellhammer T, and Kim C-J, 2002 *Sensors Actuators* **95** 259.
[6] Mugele F and Baret J-C 2005 *J. Phys.: Condens. Matter*, **17**, R705.
[7] Vallet M, Vallarde M, and Berge B 1999 *Eur. Phys. J. B* **11** 583; Verheijen HJJ and Prins MWJ 1999 *Langmuir* **15** 6616; Quinn A, Sedev R, and Ralston J 2005 *J. Phys Chem. B* **109** 6268.
[8] Jones TB 2005 *J. Micromech. Microengrg.* **15**, 1184.
[9] Pellat H 1895 *C. R. Acad. Sci. Paris* **119** 691.
[10] Jones TB, Wang K-L, and Yao D-J 2004 *Langmuir* **20** 2813.
[11] Wang K-L and Jones TB 2004 *J. Micromech. Microengrg.* **14** 761.
[12] Jones TB, Gunji M, Washizu M, and Feldman, MJ 2001 *J. Appl. Phys.* **89** 1441; Ahmed R and Jones TB 2006 *J. Electrostatics* **64**, 543.
[13] Lord Rayleigh 1945 (republication) *The Theory of Sound* (New York: Dover Press) §359.
[14] Schiaffino S and Sonin AA 1997 *J. Fluid Mech.* **343**, 95.
[15] Ahmed R, Tombs TN and Jones TB Using dielectrophoresis to control the flow of insulating liquids 2006 *Fifth Intl. Conf. on Electrowetting*: (Rochester, NY, USA, May/June 2006).